Available online at www.sciencedirect.com
SCIENCE DIRECT®
Journal of Computational Physics 192 (2003) 365–386
JOURNAL OF COMPUTATIONAL PHYSICS
www.elsevier.com/locate/jcp

A characteristic-wise hybrid compact-WENO scheme for solving hyperbolic conservation laws

Yu-Xin Ren [a,*], Miao'er Liu [a], Hanxin Zhang [b]

[a] *Department of Engineering Mechanics, Tsinghua University, Beijing 100084, PR China*
[b] *National Key Laboratory for CFD, Beijing 100083, PR China*

Received 25 February 2003; received in revised form 17 June 2003; accepted 17 July 2003

Abstract

This paper presents a fifth-order conservative hybrid compact-WENO scheme for shock-capturing calculation. The hybrid scheme is considered as the weighted average of two sub-schemes: the conservative compact scheme proposed by Pirozzoli and the WENO scheme. The weight function is designed so that the abrupt transition from one sub-scheme to another is avoided and the resulting hybrid scheme is essentially oscillation free near the flow discontinuities. A Roe type, characteristic-wise finite difference scheme is proposed which generalizes the hybrid scheme for the scalar equation to the system of conservation laws. Several test cases are presented to validate the proposed scheme.

AMS: 65M06; 76N15; 35L65

Keywords: Compact scheme; WENO scheme; Hybrid scheme; Shock-capturing; High-order scheme; Conservation laws

1. Introduction

In the DNS (direct numerical simulation) and LES (large eddy simulation) of turbulence as well as CAA (computational aero-acoustics) applications, it is required that the numerical schemes be highly accurate and capable of resolving a very broad range of length scales. If the flow fields involve shock waves, these schemes should also be essentially oscillation free near the discontinuities. In recent years, many efforts have been devoted to the development of high resolution shock-capturing schemes that are higher order accurate in smooth regions.

One class of numerical schemes among them are higher order ENO [8] and WENO [9] schemes. Such schemes have demonstrated very promising shock-capturing capabilities. However, numerical tests indicate that these schemes are usually not optimal for computing turbulent flows and aero-acoustic fields because

* Corresponding author. Tel.: +86-10-62785543; fax: +86-10-62781824.
E-mail address: ryx@tsinghua.edu.cn (Y.-X. Ren).

0021-9991/$ - see front matter
doi:10.1016/j.jcp.2003.07.006

they can lead to a significant damping of the turbulent or acoustic fluctuations. Recently, there have been attempts to improve the dissipation properties of ENO and WENO schemes. Balsara and Shu [2] have proposed the MPWENO (monotonicity preserving WENO) scheme that is up to 11th-order accurate in space. Garnier et al. [7] have used the dissipative part of the ENO scheme as a filter to regularize the solution obtained by a non-dissipative scheme.

The compact schemes are very accurate in smooth regions with spectral-like resolution, but they have been found to cause non-physical oscillations when they are applied directly to flow with discontinuities. The non-physical oscillations (Gibbs phenomena) do not decay in magnitude when the grid is refined. Such oscillations are usually unacceptable if an accurate solution is required, such as for direct numerical simulation of turbulence flow with shock waves. Several approaches have been proposed to overcome this difficulty. In order to suppress the spurious oscillation and the nonlinear instability, Cockburn and Shu [4] developed the nonlinearly stable compact schemes for shock calculations. They employed a TVB limiter to stabilize compact schemes while maintaining the formal accuracy of the scheme. Other nonlinear compact schemes can be found in papers of Deng and Maekawa [5], Deng and Zhang [6], and Wang and Huang [14]. In these papers, certain flux splitting or flux difference splitting shock-capturing schemes are incorporated with the compact schemes to avoid the spurious oscillation and to achieve higher order of accuracy.

An alternative approach is to develop so-called hybrid methods in which the non-oscillatory shock-capturing schemes are only used locally near the discontinuities and the compact schemes are used in smooth regions. Adams and Shariff [1] have proposed the hybrid compact-ENO schemes that couples a non-conservative compact upwind scheme with a shock-capturing ENO scheme that is turned on only around discontinuities. Pirozzoli [10] has derived a hybrid compact-WENO scheme in which a conservative compact scheme is developed to couple with the WENO scheme. The use of the conservative compact scheme not only facilitates the coupling with the WENO scheme that is conservative in nature but also makes the overall scheme to be conservative no matter what boundary closure scheme is adopted. According to this paper, it is shown that the overall performance of the hybrid schemes is critically affected by the order of accuracy of the shock-capturing scheme that is employed. The WENO scheme therefore represents a better candidate than the ENO scheme, as it yields better accuracy properties virtually at the same price. As a result, the conservative hybrid compact-WENO scheme in general outperforms the hybrid compact-ENO scheme of Adams and Shariff [1]. Nevertheless, both the hybrid compact-ENO scheme and the hybrid compact-WENO scheme combine the advantages of the compact schemes in smooth regions with a sharp representation of discontinuities. Another advantage of the hybrid methods is that they are computationally more efficient than other nonlinear compact schemes since the computationally expensive non-oscillatory shock-capturing schemes are used only in regions containing the discontinuities.

In the present paper, the hybrid compact-WENO scheme proposed in [10] is improved in several aspects. The hybrid schemes [1,10] may switch abruptly from one sub-scheme (e.g., the compact scheme) to another sub-scheme (e.g., ENO/WENO scheme) at the interfaces between the smooth regions and the discontinuities. Some spurious waves might be generated at these interfaces, and these spurious waves would eventually propagate into the smooth regions, as reported in [1]. In this paper,we consider the hybrid scheme as the weighted average of two sub-schemes: the conservative compact scheme proposed by Pirozzoli [10] and the WENO scheme. The weight function is designed to be continuous so that the abrupt transition from one sub-scheme to another is avoided. When solving a system of hyperbolic conservation laws such as the Euler equations of gas dynamics, Pirozzoli [10] used the Lax–Friedrichs flux splitting to split the fluxes into positive part and negative part and the numerical flux functions were evaluated in a component by component manner. Although this approach is quite simple and efficient, its resolution power is not as good as the characteristic decomposition approach, and it can cause an excessive smearing of the shear waves. In the present paper, a characteristic-wise hybrid compact-WENO scheme is proposed which couples the Roe type, characteristic-wise compact sub-scheme and the Roe type characteristic-wise WENO scheme proposed by Jiang and Shu [9]. In order to remove the entropy violating solutions and the

shock instabilities such as the "carbuncle" and the "odd-even decoupling" phenomena associated with the Roe type scheme, an improved entropy fix procedure based on the "H-correction" [11] is adopted . For the present characteristic-wise hybrid compact-WENO scheme, when evaluating the flux functions of a system of conservation laws, we need to solve one or more block-tridiagonal systems of linear equations rather than tridiagonal systems of linear equations. Therefore, the present scheme is computationally more expensive than the Pirozzoli [10] scheme. However, numerical tests show a significant improvement in resolution for flows with complex structures.

The paper is organized as follows. In Section 2, the hybrid compact-WENO scheme is formulated for the scalar conservation law , and the design and the performance of the weight functions are discussed. In Section 3, the characteristic-wise hybrid compact-WENO scheme for the Euler equations of gas dynamics is presented. In Section 4, the hybrid scheme is applied to a number of benchmark test cases. The conclusion remarks are given in Section 5.

2. The hybrid compact-WENO scheme for scalar conservation laws

2.1. The governing equation and the finite difference scheme

Consider the scalar hyperbolic conservation law given by

$$\frac{\partial u}{\partial t}+\frac{\partial f}{\partial x}=0 \tag{1}$$

with proper initial and boundary conditions, where $f=f(u)$. By the hyperbolicity of Eq. (1), $\partial f/\partial u$ is a real function of u. Let $\{I_j\}$ be a uniform partition of the solution domain in space, where $I_j=[x_{j-1/2},x_{j+1/2}]$ and $x_{j+1/2}-x_{j-1/2}=h$. The semi-discrete conservative finite difference scheme of Eq. (1) can be written as

$$\frac{\partial u_j}{\partial t}+\frac{1}{h}\left(\hat{f}_{j+1/2}-\hat{f}_{j-1/2}\right)=0, \tag{2}$$

where $\hat{f}_{j+1/2}$ is the numerical flux function. If

$$\frac{1}{h}\left(\hat{f}_{j+1/2}-\hat{f}_{j-1/2}\right)=\left(\frac{\partial f}{\partial x}\right)_j+\mathrm{O}(h^k), \tag{3}$$

this scheme is kth order accurate in space.

In the present work, the time integration is performed by means of a three-stage, TVD Runge–Kutta scheme [13]. Defining

$$L_j(u)=-\frac{1}{h}\left(\hat{f}_{j+1/2}-\hat{f}_{j-1/2}\right),$$

then this scheme is given by

$$u_j^{(1)}=u_j^n+\Delta t L_j(u^n),$$

$$u_j^{(2)}=\frac{3}{4}u_j^n+\frac{1}{4}u_j^{(1)}+\frac{1}{4}\Delta t L_j(u^{(1)}),$$

$$u_j^{n+1}=\frac{1}{3}u_j^n+\frac{2}{3}u_j^{(2)}+\frac{2}{3}\Delta t L_j(u^{(2)}).$$

2.2. The conservative upwind compact scheme

For $k = 5$ in Eq. (3), the numerical flux function in Eq. (2) can be computed by using the fifth-order conservative upwind compact scheme proposed by Pirozzoli [10]:

$$\frac{1}{2}\hat{f}_{j-1/2} + \hat{f}_{j+1/2} + \frac{1}{6}\hat{f}_{j+3/2} = \frac{1}{18}f_{j-1} + \frac{19}{18}f_j + \frac{5}{9}f_{j+1} \quad \text{if } \tilde{a}_{j+1/2} \geqslant 0, \tag{4a}$$

$$\frac{1}{6}\hat{f}_{j-1/2} + \hat{f}_{j+1/2} + \frac{1}{2}\hat{f}_{j+3/2} = \frac{5}{9}f_j + \frac{19}{18}f_{j+1} + \frac{1}{18}f_{j+2} \quad \text{if } \tilde{a}_{j+1/2} < 0, \tag{4b}$$

where $\tilde{a}_{j+1/2}$ is the numerical wave speed defined by

$$\tilde{a}_{j+1/2} = \begin{cases} \frac{\hat{f}_{j+1} - \hat{f}_j}{u_{j+1} - u_j} & \text{if } u_{j+1} - u_j \neq 0, \\ \left(\frac{\partial f}{\partial u}\right)_j, & \text{otherwise.} \end{cases}$$

Denoting $s_{j+1/2} = \text{sign}(\tilde{a}_{j+1/2})$, Eqs. (4a) and (4b) can be combined into a unified form:

$$\phi_{j+1/2}\hat{f}_{j-1/2} + \hat{f}_{j+1/2} + \psi_{j+1/2}\hat{f}_{j+3/2} = \hat{b}_{j+1/2}, \tag{5}$$

where

$$\phi_{j+1/2} = \frac{1}{3} + \frac{s_{j+1/2}}{6}, \quad \psi_{j+1/2} = \frac{1}{3} - \frac{s_{j+1/2}}{6},$$

and

$$\hat{b}_{j+1/2} = \left(\frac{1 + s_{j+1/2}}{2}\right)\left(\frac{1}{18}f_{j-1} + \frac{19}{18}f_j + \frac{5}{9}f_{j+1}\right) + \left(\frac{1 - s_{j+1/2}}{2}\right)\left(\frac{5}{9}f_j + \frac{19}{18}f_{j+1} + \frac{1}{18}f_{j+2}\right).$$

The order of accuracy and the dispersion/dissipation properties of Eq. (5) have been discussed in detail in [10] and will not be repeated here. In the present paper, we also use the same boundary schemes corresponding to Eq. (5) that have been reported in [10].

2.3. The WENO scheme

The numerical flux function in Eq. (2) can also be evaluated by the fifth-order finite difference WENO scheme of Jiang and Shu [9]. For completeness, the formulations of this WENO scheme will be given as follows.

The numerical flux function of the fifth-order WENO scheme can be expressed as

$$\hat{f}^{\text{WENO}}_{j+1/2} = \sum_{\gamma=0}^{2} \omega_\gamma f^\gamma_{j+1/2},$$

where $f^\gamma_{j+1/2}$ is obtained by a second-order polynomial reconstruction of $f(u(x_{j+1/2}))$ on γth set of candidate stencils S_γ. For $\gamma = 0$, 1, and 2, S_γ will cover all possible stencils including the grid point that one point upwind to $x_{j+1/2}$. For each γ, ω_γ is the weight that satisfies the condition

$$\omega_\gamma \geqslant 0, \quad \sum_{\gamma=0}^{2} \omega_\gamma = 1.$$

In [9], ω_γ is computed using

$$\omega_\gamma = \frac{d_\gamma}{(\epsilon+\beta_\gamma)^2} \Big/ \sum_{l=0}^{2} \frac{d_l}{(\epsilon+\beta_l)^2},$$

where d_γ is a coefficient that guarantees the overall scheme is fifth-order accurate in space, β_γ is the smoothness indicator and ϵ is a small positive number to avoid divisions by zero. For $\tilde{a}_{j+1/2} \geqslant 0$, we have $d_0 = 0.3$, $d_1 = 0.6$, and $d_2 = 0.1$. And $f^\gamma_{j+1/2}$, β_γ $(\gamma = 0, 1, 2)$ can be computed, respectively, by

$$f^0_{j+1/2} = \frac{1}{3}f_j + \frac{5}{6}f_{j+1} - \frac{1}{6}f_{j+2},$$

$$f^1_{j+1/2} = -\frac{1}{6}f_{j-1} + \frac{5}{6}f_j + \frac{1}{3}f_{j+1},$$

$$f^2_{j+1/2} = \frac{1}{3}f_{j-2} - \frac{7}{6}f_{j-1} + \frac{11}{6}f_j$$

and

$$\beta_0 = \frac{13}{12}(f_j - 2f_{j+1} + f_{j+2})^2 + \frac{1}{4}(3f_j - 4f_{j+1} + f_{j+2})^2,$$

$$\beta_1 = \frac{13}{12}(f_{j-1} - 2f_j + f_{j+1})^2 + \frac{1}{4}(f_{j-1} - f_{j+1})^2,$$

$$\beta_2 = \frac{13}{12}(f_{j-2} - 2f_{j-1} + f_j)^2 + \frac{1}{4}(f_{j-2} - 4f_{j-1} + 3f_j)^2.$$

For $\tilde{a}_{j+1/2} < 0$, we have $d_0 = 0.1$, $d_1 = 0.6$, and $d_2 = 0.3$. The formulations for $f^\gamma_{j+1/2}$, β_γ $(\gamma = 0, 1, 2)$ become

$$f^0_{j+1/2} = \frac{11}{6}f_{j+1} - \frac{7}{6}f_{j+2} + \frac{1}{3}f_{j+3},$$

$$f^1_{j+1/2} = \frac{1}{3}f_j + \frac{5}{6}f_{j+1} - \frac{1}{6}f_{j+2},$$

$$f^2_{j+1/2} = -\frac{1}{6}f_{j-1} + \frac{5}{6}f_j + \frac{1}{3}f_{j+1}$$

and

$$\beta_0 = \frac{13}{12}\left(f_{j+1} - 2f_{j+2} + f_{j+3}\right)^2 + \frac{1}{4}\left(3f_{j+1} - 4f_{j+2} + f_{j+3}\right)^2,$$

$$\beta_1 = \frac{13}{12}\left(f_j - 2f_{j+1} + f_{j+2}\right)^2 + \frac{1}{4}\left(f_j - f_{j+2}\right)^2,$$

$$\beta_2 = \frac{13}{12}\left(f_{j-1} - 2f_j + f_{j+1}\right)^2 + \frac{1}{4}\left(f_{j-1} - 4f_j + 3f_{j+1}\right)^2.$$

2.4. The hybrid compact-WENO scheme

The compact scheme given in Eq. (5) gives very satisfactory results if the solution is smooth everywhere. However, the Gibbs phenomena will occur when there are discontinuities in the solution. The Gibbs phenomena will contaminate the solution and may lead to nonlinear instability. In order to cure this deficiency, the hybrid schemes have been proposed [1,10] in which the compact scheme is coupled with the ENO or WENO scheme. As a result, in the hybrid method, the compact scheme is applied segment by segment in the smooth regions. Near the discontinuities that separate the smooth regions, the ENO/WENO scheme is used instead. Theoretically, this is a quite natural approach since by its derivation, the linear compact scheme assumes the global smoothness of the solution and therefore cannot be applied across the discontinuities where the shock-capturing schemes are necessary in order to suppress the non-physical oscillations. In the present paper, we consider the hybrid scheme as the weighted average of two sub-schemes: the conservative compact scheme presented in Section 2.2 and the WENO [9] scheme. This scheme can be written in the following form:

$$\sigma_{j+1/2}\phi_{j+1/2}\hat{f}_{j-1/2} + \hat{f}_{j+1/2} + \sigma_{j+1/2}\psi_{j+1/2}\hat{f}_{j+3/2} = \hat{c}_{j+1/2}, \tag{6}$$

where $\sigma_{j+1/2}$ is the weight and

$$\hat{c}_{j+1/2} = \sigma_{j+1/2}\hat{b}_{j+1/2} + (1-\sigma_{j+1/2})\hat{f}^{\mathrm{WENO}}_{j+1/2}.$$

Eq. (6) will reduce to the compact scheme if $\sigma_{j+1/2} = 1$ and to the WENO scheme if $\sigma_{j+1/2} = 0$. According to the spirit of the hybrid scheme, it is necessary that the weight be directly related to the smoothness of the numerical solution. Therefore, a smoothness indicator $r_{j+1/2}$ must be defined and the weight should be a function of $\{r_{j+1/2}\}$. In [10], the smoothness indicator is simply defined to be $r_{j+1/2} = |f_{j+1} - f_j|$, and $\sigma_{j+1/2}$ is determined by

$$\sigma_{j+1/2} = \begin{cases} 1 & \text{if } r_{j-1/2} \leqslant \tilde{r}_c \text{ and } r_{j+1/2} \leqslant \tilde{r}_c \text{ and } r_{j+3/2} \leqslant \tilde{r}_c, \\ 0, & \text{otherwise,} \end{cases} \tag{7}$$

where $\tilde{r}_c$ is a threshold value that is usually problem-dependent. This smoothness indicator and the corresponding weight produce very good numerical results [1,10]. However, using the weight in Eq. (7), the hybrid scheme may switch abruptly from one sub-scheme to another sub-scheme at the interfaces between the smooth regions and the discontinuities.

In the present paper, the smoothness indicator is designed to be

$$r_{j+1/2} = \min(r_j, r_{j+1}), \tag{8}$$

where

$$r_j = \frac{|2\Delta f_{j+1/2}\Delta f_{j-1/2}| + \varepsilon}{(\Delta f_{j+1/2})^2 + (\Delta f_{j-1/2})^2 + \varepsilon}, \tag{9}$$

and $\Delta f_{j+1/2} = f_{j+1} - f_j$. The ε is a positive real number to avoid possible division by zero. It is apparent that $r_{j+1/2} \in [0,1]$ and this will facilitate the choice of the threshold value r_c (see Eq. (11)). We note that other forms of the smoothness indicator have also been used in [7,16]. In order to avoid the non-smooth transition between the sub-schemes, the weight can be defined as a smooth function of the smoothness indicator. A very simple choice is

$$\sigma_{j+1/2} = r_{j+1/2}. \tag{10}$$

This weight is very robust and produces numerical results without spurious oscillations. However, the resulting hybrid scheme is less efficient than using Eq. (7) because the WENO scheme is needed everywhere. On the other hand, when using Eq. (7), the WENO scheme is applied only at places where $\sigma = 0$. Numerical

tests also indicate that the hybrid scheme using this weight is slightly more dissipative than that using Eq. (7) with a proper choice of $\tilde{r}_c$. To make a compromise between the robustness and the efficiency as well as accuracy, we suggest that the weight be a continuous rather than a smooth function of the smoothness indicator that takes the following form:

$$\sigma_{j+1/2} = \min\left(1, \frac{r_{j+1/2}}{r_c}\right). \tag{11}$$

In this case, the WENO scheme is not needed when $\sigma = 1$ and when a smaller threshold value r_c is chosen, the hybrid scheme will become less dissipative. For the purpose of future reference, we denote the weight defined in Eqs. (7) and (11), respectively, by *Weight A* and *Weight B*. We note Weight B will reduce to the weight in Eq. (10) when $r_c = 1$.

Remark. In the LES and DNS of turbulence flows, there is a possibility that in Eq. (9), both $|\Delta f_{j+1/2}|$ and $|\Delta f_{j-1/2}|$ are physically very small due to turbulent fluctuations but their ratio $|\Delta f_{j+1/2}|/|\Delta f_{j-1/2}|$ is much larger or smaller than unity. In this case, the smoothness indicator Eq. (8) will be very small and the weight of the more dissipative WENO sub-scheme is likely to be larger than that of the compact sub-scheme at the interface $j + 1/2$. For Weight B, this shortcoming can be easily overcome by a proper design of ε in Eq. (9). In this paper, we choose

$$\varepsilon = \frac{0.9 r_c}{1 - 0.9 r_c}\xi^2, \tag{12}$$

where ξ is a user specified positive number. It can be easily verified that when

$$\max(|\Delta f_{j-1/2}|, |\Delta f_{j+1/2}|, |\Delta f_{j+3/2}|) \leqslant \xi,$$

we always have

$$\sigma_{j+1/2} \geqslant 0.9$$

and therefore the compact sub-scheme will dominate the hybrid scheme . It is also clear that ξ acts as a threshold value. All fluctuations smaller than this value will be considered as turbulent fluctuations and will not be damped by using the WENO scheme. In the present paper, only the inviscid flow is simulated. The value of ξ is therefore set arbitrarily to 10^{-3}.

2.5. The performance of weight functions

In order to test the performance of these weight functions, the hybrid compact-WENO (Eq. (5)) is applied to solve the linear advection equation

$$\frac{\partial u}{\partial t} + \frac{\partial u}{\partial x} = 0$$

numerically using Weight A and Weight B, respectively. The initial conditions are

$$u(x,0) = \begin{cases} 1, & -1 \leqslant x < -0.5, \\ \sin[\pi(x + 0.5)], & -0.5 \leqslant x < 0.5, \\ 1, & 0.5 \leqslant x \leqslant 1, \end{cases} \tag{13}$$

and the periodic boundary conditions are used at $x = \pm 1$. The solution has been computed on $N = 100$ uniform grids using a Courant number CFL $= 0.5$.

The numerical results at $t = 2$ are shown in Fig. 1. Specifically, Fig. 1(a) shows the results obtained using Weight A with $\tilde{r}_c = 0.1$ and $\tilde{r}_c = 0.3$. It is clear that the scheme predicts the solution very accurately in the

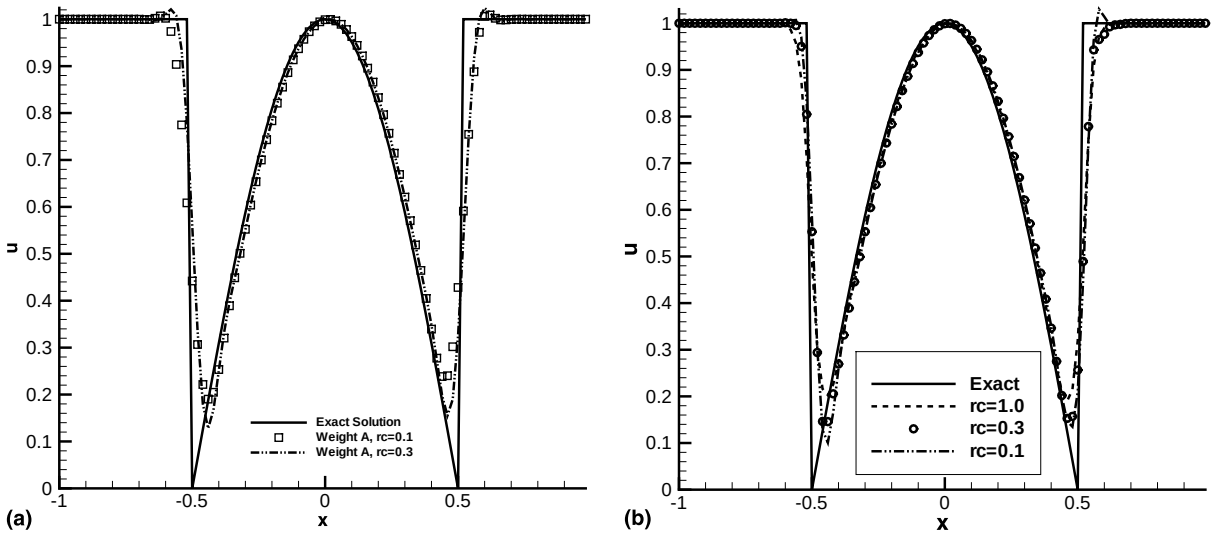

Fig. 1. A comparison between the numerical results using different weight functions: (a) Weight A, (b) Weight B.

smooth regions and the discontinuities can be captured in high resolution. However, the numerical oscillations are observed near the discontinuities. Fig. 1(b) reports the numerical results using Weight B and the threshold value r_c is chosen as 1.0, 0.3, and 0.1, respectively. It can be seen that with the decrease of r_c, higher resolution can be achieved. The numerical result produced by using Weight B with $r_c = 0.3$ is in similar resolution to that produced by using Weight A with $\tilde{r}_c = 0.3$. However, no numerical oscillations occur using Weight B. Generally speaking, there is a lower bound of r_c in Weight B that will produce an oscillation-free solution. No theoretical result is currently available for this lower bound and it has to be determined through numerical experiments. In the present test case, this lower bound is around 0.2 according to the numerical experiments. It can be concluded from this comparison that Weight B with a proper choice of r_c (that is in general problem dependent) yields the overall best numerical results. In the following sections, we choose Weight B only as the weight function in the hybrid scheme.

To illustrate the behavior of the weight function more clearly, we have also performed the static reconstruction to Eq. (13). The distributions of the weight functions with $r_c = 1$, $r_c = 0.3$, and $r_c = 0.1$ are plotted in Fig. 2. Near the discontinuities, the weights are smaller than unity and the WENO scheme will be invoked at these interfaces. The width of the degeneracy is around 2–3 points depending on the value of r_c. When $r_c = 0.3$ and $r_c = 0.1$, we have $\sigma = 1$ in smooth regions. However, when $r_c = 1$ is used, the degeneracy also happens in the smooth region near the extremum. This fact explains why the hybrid scheme will become more dissipative when a larger threshold value r_c is chosen.

3. The hybrid compact-WENO scheme for the Euler equations of gas dynamics

3.1. The Euler equations of gas dynamics

In this section, the hybrid compact-WENO scheme will be extended to solve systems of hyperbolic conservation laws. Specifically, we are interested in the Euler equations of gas dynamics which, in one-dimensional case, can be written in the following conservation form:

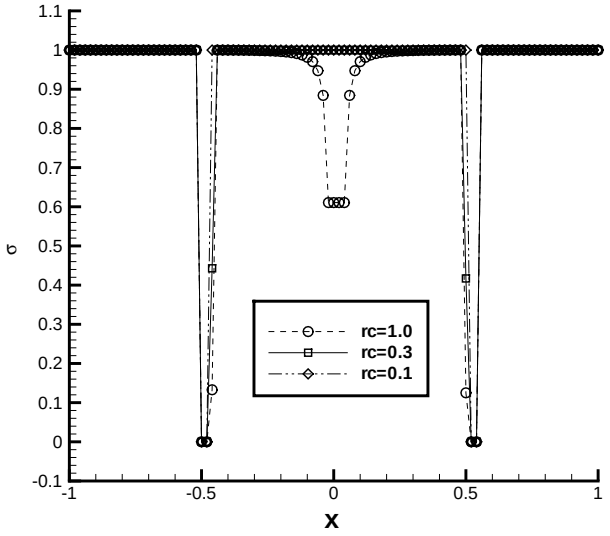

Fig. 2. The σ–x distribution of Weight B with $r_c = 1$, $r_c = 0.3$, and $r_c = 0.1$.

$$\frac{\partial \mathbf{U}}{\partial t} + \frac{\partial \mathbf{F}}{\partial x} = \mathbf{0}, \tag{14}$$

where

$$\mathbf{U} = \begin{bmatrix} \rho \\ \rho u \\ \rho E \end{bmatrix}, \quad \mathbf{F} = \begin{bmatrix} \rho u \\ \rho u^2 + p \\ \rho u H \end{bmatrix},$$

$H = E + p/\rho$ is the enthalpy. This set of equations are closed by the equation-of-state of ideal gas

$$p = (\gamma - 1)\rho(E - u^2/2).$$

For Eq. (14), the Jacobian matrix $A = \frac{\partial \mathbf{F}}{\partial \mathbf{U}}$ has three real eigenvalues

$$\lambda^{(1)} = u - a, \quad \lambda^{(2)} = a, \quad \lambda^{(3)} = u + a,$$

where $a = (\frac{\gamma p}{\rho})^{1/2}$ is the speed of sound and a complete set of independent right eigenvectors

$$\mathbf{r}^{(1)} = \begin{bmatrix} 1 \\ u - a \\ H - ua \end{bmatrix}, \quad \mathbf{r}^{(2)} = \begin{bmatrix} 1 \\ u \\ u^2/2 \end{bmatrix}, \quad \mathbf{r}^{(3)} = \begin{bmatrix} 1 \\ u + a \\ H + ua \end{bmatrix}. \tag{15}$$

We denote the matrix whose columns are eigenvectors in Eq. (15) by

$$R = (\mathbf{r}^{(1)}, \mathbf{r}^{(2)}, \mathbf{r}^{(3)}),$$

and denote $L = R^{-1}$. Then it is easy to show

$$LAR = \Lambda,$$

where Λ is the diagonal matrix $\Lambda = \mathrm{diag}(\lambda^{(1)}, \lambda^{(2)}, \lambda^{(3)})$. Notice the row vectors of L, denoted by $\mathbf{l}^{(1)}, \mathbf{l}^{(2)}, \mathbf{l}^{(3)}$ are left eigenvectors of A:

$$\mathbf{l}^{(i)} A = \lambda^{(i)} \mathbf{l}^{(i)}, \quad i = 1, 2, 3.$$

3.2. The finite difference scheme

As in the scalar case, the semi-discrete conservative finite difference scheme of Eq. (14) can be written as

$$\frac{\partial \mathbf{U}_j}{\partial t} + \frac{1}{h}\left(\hat{\mathbf{F}}_{j+1/2} - \hat{\mathbf{F}}_{j-1/2}\right) = 0, \tag{16}$$

where $\hat{\mathbf{F}}_{j+1/2}$ is the numerical flux function. In this section, we are going to design the spatially fifth-order finite difference equations for the Euler equations that satisfying

$$\frac{1}{h}\left(\hat{\mathbf{F}}_{j+1/2} - \hat{\mathbf{F}}_{j-1/2}\right) = \left(\frac{\partial \mathbf{F}}{\partial x}\right)_j + \mathrm{O}(h^5).$$

The time integration is performed again by means of a three-stage, TVD Runge–Kutta scheme similar to the scalar case.

3.3. The hybrid compact-WENO scheme for the Euler equations

When solving the Euler equations, Pirozzoli [10] used the Lax–Friedrichs flux splitting to split the fluxes into positive part and negative part. The resulting hybrid scheme solves the Euler equations in a component by component manner. This approach works reasonably well for many problems. However, for more demanding test problems, it is usually advisable to use the more costly but much sounder approach based on the characteristic decompositions [12]. In the present paper, a characteristic-wise hybrid compact-WENO scheme is proposed which couples the Roe type, characteristic-wise compact sub-scheme with the characteristic-wise WENO sub-scheme proposed by Jiang and Shu [9]. The evaluation of the numerical flux functions for the characteristic-wise hybrid compact-WENO scheme consists the following steps:

1. At each fixed $x_{j+1/2}$, the average state $\mathbf{U}_{j+1/2}$ is computed by the simple mean

$$\mathbf{U}_{j+1/2} = \frac{1}{2}\left(\mathbf{U}_j + \mathbf{U}_{j+1}\right),$$

   or the Roe average.
2. The eigenvalues $\lambda^{(i)}_{j+1/2}$ $(i = 1, 2, 3)$ and the left eigenvectors $\mathbf{l}^{(i)}_{j+1/2}$ $(i = 1, 2, 3)$ are computed in terms of $\mathbf{U}_{j+1/2}$.
3. The local characteristic decompositions of the flux functions at x_m $(m = j-1, \ldots, j+2)$ are computed using

$$w^{(i)}_m = \mathbf{l}^{(i)}_{j+1/2}\mathbf{F}_m, \quad i = 1, 2, 3; \;\; m = j-1, \ldots, j+2.$$

4. By defining

$$s^{(i)}_{j+1/2} = \mathrm{sign}\left(\lambda^{(i)}_{j+1/2}\right),$$

$$r^{(i)}_{j+1/2} = \min\left(r^{(i)}_j, r^{(i)}_{j+1}\right),$$

$$r^{(i)}_j = \frac{|2\Delta w^{(i)}_{j+1/2}\Delta w^{(i)}_{j-1/2}| + \varepsilon}{\left(\Delta w^{(i)}_{j+1/2}\right)^2 + \left(\Delta w^{(i)}_{j-1/2}\right)^2 + \varepsilon},$$

and

$$\sigma_{j+1/2}^{(i)} = \min\left(1, \frac{r_{j+1/2}^{(i)}}{r_c}\right)$$

for $i = 1$, 2, and 3, the hybrid compact-WENO scheme for the scalar equation (Eq. (5)) can be applied to the local characteristic variables $w^{(i)}$ $(i = 1, 2, 3)$ as

$$\sigma_{j+1/2}^{(i)}\phi_{j+1/2}^{(i)}\hat{w}_{j-1/2}^{(i)} + \hat{w}_{j+1/2}^{(i)} + \sigma_{j+1/2}^{(i)}\psi_{j+1/2}^{(i)}\hat{w}_{j+3/2}^{(i)} = \hat{c}_{j+1/2}^{(i)}, \tag{17}$$

where

$$\phi_{j+1/2}^{(i)} = \frac{1}{3} + \frac{s_{j+1/2}^{(i)}}{6}, \quad \psi_{j+1/2}^{(i)} = \frac{1}{3} - \frac{s_{j+1/2}^{(i)}}{6},$$

$$\hat{c}_{j+1/2}^{(i)} = \sigma_{j+1/2}^{(i)}\hat{b}_{j+1/2}^{(i)} + \left(1 - \sigma_{j+1/2}^{(i)}\right)\hat{w}_{j+1/2}^{(i),\mathrm{WENO}}, \tag{18}$$

and

$$\hat{b}_{j+1/2}^{(i)} = \left(\frac{1 + s_{j+1/2}^{(i)}}{2}\right)\left(\frac{1}{18}w_{j-1}^{(i)} + \frac{19}{18}w_j^{(i)} + \frac{5}{9}w_{j+1}^{(i)}\right) + \left(\frac{1 - s_{j+1/2}^{(i)}}{2}\right)\left(\frac{5}{9}w_j^{(i)} + \frac{19}{18}w_{j+1}^{(i)} + \frac{1}{18}w_{j+2}^{(i)}\right),$$

$\hat{w}_{j+1/2}^{(i),\mathrm{WENO}}$ in Eq. (18) is computed using the characteristic-wise finite difference WENO scheme of Roe type [9,12]. It should be noted that for fixed i, Eq. (17) cannot be solved directly since the $\hat{w}_{j+1/2}^{(i)}$ is defined locally. In the following step, Eq. (17) for all characteristic fields will be arranged in to a block-tridiagnal system of equations that can be solved to obtain the numerical flux in the physical space.

5. For $i = 1$, 2, and 3, Eq. (17) can be written as

$$\Phi_{j+1/2}\hat{\mathbf{F}}_{j-1/2} + L_{j+1/2}\hat{\mathbf{F}}_{j+1/2} + \Psi_{j+1/2}\hat{\mathbf{F}}_{j+3/2} = \hat{\mathbf{c}}_{j+1/2}, \tag{19}$$

where

$$\Phi_{j+1/2} = \begin{bmatrix} \sigma_{j+1/2}^{(1)}\phi_{j+1/2}^{(1)}\mathbf{l}_{j+1/2}^{(1)} \\ \sigma_{j+1/2}^{(2)}\phi_{j+1/2}^{(2)}\mathbf{l}_{j+1/2}^{(2)} \\ \sigma_{j+1/2}^{(3)}\phi_{j+1/2}^{(3)}\mathbf{l}_{j+1/2}^{(3)} \end{bmatrix},$$

$$L_{j+1/2} = \begin{bmatrix} \mathbf{l}_{j+1/2}^{(1)} \\ \mathbf{l}_{j+1/2}^{(2)} \\ \mathbf{l}_{j+1/2}^{(3)} \end{bmatrix},$$

$$\Psi_{j+1/2} = \begin{bmatrix} \sigma_{j+1/2}^{(1)}\psi_{j+1/2}^{(1)}\mathbf{l}_{j+1/2}^{(1)} \\ \sigma_{j+1/2}^{(2)}\psi_{j+1/2}^{(2)}\mathbf{l}_{j+1/2}^{(2)} \\ \sigma_{j+1/2}^{(3)}\psi_{j+1/2}^{(3)}\mathbf{l}_{j+1/2}^{(3)} \end{bmatrix},$$

and

$$\hat{\mathbf{c}}_{j+1/2} = \begin{bmatrix} \hat{c}_{j+1/2}^{(1)} \\ \hat{c}_{j+1/2}^{(2)} \\ \hat{c}_{j+1/2}^{(3)} \end{bmatrix}.$$

Clearly, Eq. (19) and additional boundary closures form a block-tridiagnal system of equations which can be solved to obtain $\hat{\mathbf{F}}_{j+1/2}$.

It is straightforward to extend the one-dimensional characteristic-wise hybrid compact-WENO scheme to the multi-dimensional cases. We omit this derivation in the present paper for brevity.

We now give some remarks concerning the implementation and the efficiency of the characteristic-wise hybrid compact-WENO scheme.

Remark 1. The WENO sub-scheme plays an important role in the hybrid scheme. We basically use the Roe type characteristic-wise WENO scheme [9] in the hybrid method. The Roe type WENO scheme is less dissipative and thus achieves higher resolution than the WENO scheme based on the flux vector splitting, which is especially true in capturing the contact discontinuities and shear layers in viscous flows. However, the Roe type WENO scheme admits rarefaction shocks that do not satisfy the entropy condition. Therefore, certain entropy fix procedure is needed. In [9], the Roe type local characteristic-wise WENO flux with entropy fix is evaluated with

$$\hat{w}_{j+1/2}^{(i),\mathrm{WENO}} = \begin{cases} \hat{w}_{j+1/2}^{(i),\mathrm{WENO-Roe}} & \text{if } \lambda_j^{(i)}\lambda_{j+1}^{(i)} > 0, \\ \hat{w}_{j+1/2}^{(i),\mathrm{WENO-LF}}, & \text{otherwise.} \end{cases} \tag{20}$$

In Eq. (20), the WENO-Roe and WENO-LF stand for the original Roe type WENO flux and WENO flux based on the Lax–Friedrich flux splitting. The detailed formulations can be found in [12] and will not be repeated here. This entropy fix procedure is very successful and always yields the correct entropy solution according to the numerical tests. However, this entropy fix procedure is not sufficient to cure the "odd-even decoupling" and the "carbuncle" phenomenon that may occur in some multi-dimensional problems involving strong normal shocks. In order to eliminate such kind of shock instabilities, we propose to use the "H-correction" procedure [11] in the framework of characteristic-wise hybrid scheme in the present paper. For two-dimensional problems, the characteristic-wise WENO flux at interface $(j+1/2,k)$ is computed according to:

$$\hat{w}_{j+1/2,k}^{(i),\mathrm{WENO}} = \begin{cases} \hat{w}_{j+1/2,k}^{(i),\mathrm{WENO-Roe}} & \text{if } \min\left(|\lambda_{j,k}^{(i)}|, |\lambda_{j+1,k}^{(i)}|\right) \geqslant \eta_{j+1/2,k}, \\ \hat{w}_{j+1/2,k}^{(i),\mathrm{WENO-LF}}, & \text{otherwise.} \end{cases} \tag{21}$$

In Eq. (21), $\eta_{j+1/2,k}$ is determined by

$$\eta_{j+1/2,k} = \max\left(\eta_{j+1/2,k}^{x}, \eta_{j,k-1/2}^{y}, \eta_{j,k+1/2}^{y}, \eta_{j+1,k-1/2}^{y}, \eta_{j+1,k+1/2}^{y}\right),$$

where

$$\eta_{j+1/2,k}^{x} = |u_{j+1,k} - u_{j,k}| + |a_{j+1,k} - a_{j,k}|,$$

$$\eta_{j,k+1/2}^{y} = |v_{j,k+1} - v_{j,k}| + |a_{j,k+1} - a_{j,k}|,$$

and $a_{j,k}$ is the speed of sound at grid point (j,k). Our numerical experiments indicate that this approach works well in removing the shock instabilities.

Remark 2. The Weight B defined in Section 2 is adopted in the hybrid scheme for Euler equations. The smoothness indicator for each characteristic field is computed in terms of local characteristic variables. Although we can use a simpler approach to evaluate the smoothness properties on the basis of the density or Mach number for all characteristic fields, superior numerical results are obtained by using the present

method. The choice of r_c in the weight is important in the hybrid scheme. When a very small r_c is chosen, the computation may break down due to negative pressure and/or density for some test cases. Numerical experiments indicate that optimal results can be obtained when r_c is chosen between 0.3 and 0.5. Theoretically, different r_c can be used for different characteristic fields, but this is not tested in the present paper and we will use the same r_c for all characteristic fields.

Remark 3. To compute the flux function $\hat{\mathbf{F}}_{j+1/2}$ in Eq. (19), we need to solve a block tridiagnal system of equations. Although there is an efficient direct method to solve this system of equations, it turns out that the characteristic-wise hybrid compact-WENO scheme is computationally more expensive than the component-wise hybrid compact-WENO scheme in which only tridiagnal systems of equations need to be solved. According to our codes, the component-wise scheme is about twice more efficient than the characteristic-wise scheme. Nevertheless, the characteristic-wise scheme can yield better numerical results than the component-wise scheme, which compensates its cost to a large extent.

4. Numerical tests

In the present section, we discuss the application of the characteristic-wise hybrid compact-WENO scheme for some benchmark cases in both one and two dimensions. For the scalar case, the present hybrid compact-WENO scheme is basically identical to the hybrid scheme of Pirozzoli [10] except that different smoothness indicator and weight function are used. Since the influences of the smoothness indicators and weight functions for the scalar equation have been studied in Section 2.5, we therefore focus on the Euler equations of gas dynamics in the present section. For all test cases, Weight B is chosen as the weight function.

4.1. Shu–Osher problem

The following test case is taken from [13]. The governing equations are the one-dimensional Euler equations and the initial conditions are

$$(\rho, u, p) = \begin{cases} (3.857143, 2.629369, 10.333333) & \text{if } x < 1, \\ (1 + 0.2\sin(5x - 5), 0, 1) & \text{if } x \geqslant 1. \end{cases}$$

Physically, this problems represents that a Mach 3 shock interacts with a density disturbance which will generate a flow field with both smooth structure and discontinuities. The solution is advanced in time up to $t = 1.8$ on the computational domain $x \in [0, 10]$. The grid number is $N = 200$. The time step is determined by

$$\Delta t = \mathrm{CFL}\frac{h}{\max_j(|u|_j + a_j)}$$

with a Courant number $\mathrm{CFL} = 0.5$. Numerical results of the density distribution computed using WENO and characteristic-wise hybrid compact-WENO scheme are shown in Fig. 3. The solid line in this figure is obtained by computing the same problem using the WENO scheme with $N = 2000$ grid points, which is considered to be the "exact" solution although the real exact solution is not known for this problem. By comparing Fig. 3(a) with Figs. 3(b)–(d), it is clear that the hybrid scheme demonstrates superior resolution over the WENO scheme in reproducing the correct flow features downstream of the shock. Specifically, the WENO scheme produces a rather poor result in predicting the post-shock entropy waves, whereas these waves can be captured more clearly using the hybrid scheme. The threshold value r_c in the weight has a

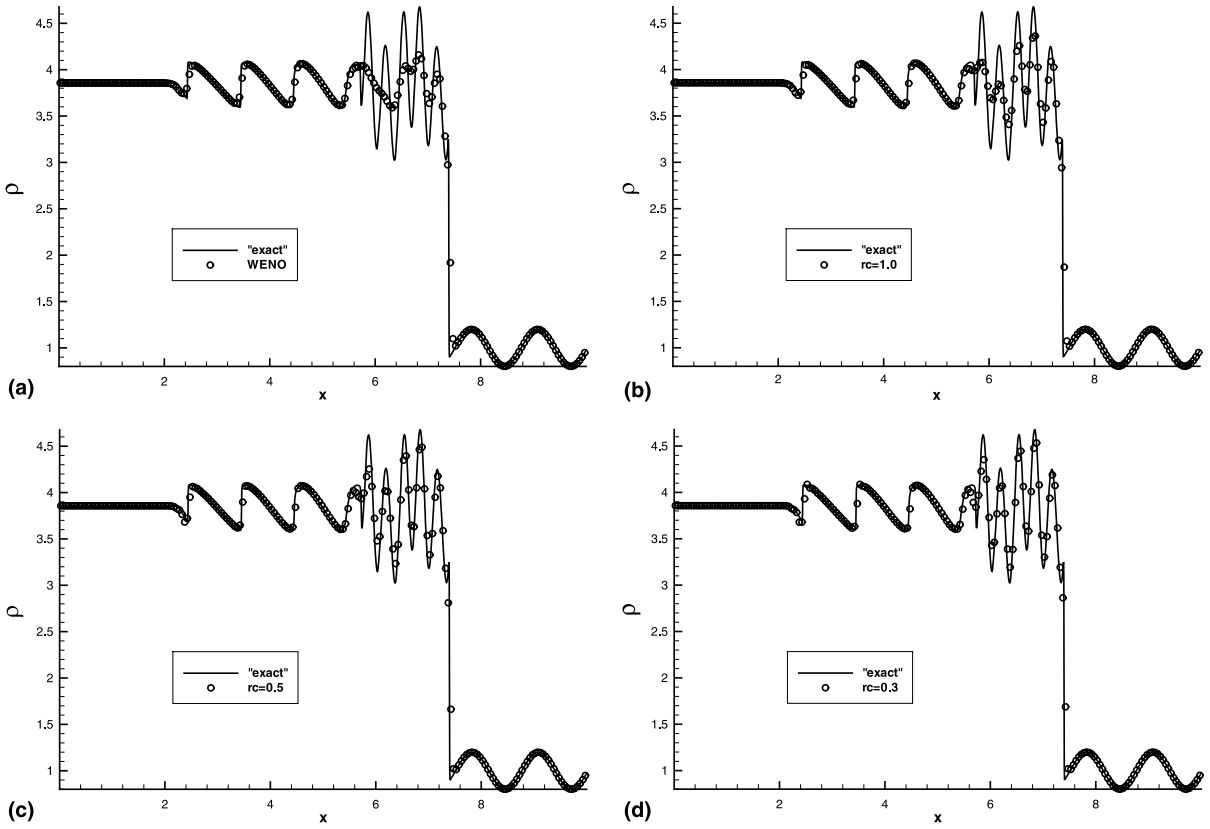

Fig. 3. Shu–Osher problem, distribution of density for $N = 200$, $t = 1.8$. (a) Characteristic-wise WENO scheme. (b) Component-wise hybrid compact-WENO scheme, $r_c = 1.0$. (c) Characteristic-wise hybrid compact-WENO scheme, $r_c = 0.5$. (d) Characteristic-wise hybrid compact-WENO scheme, $r_c = 0.3$.

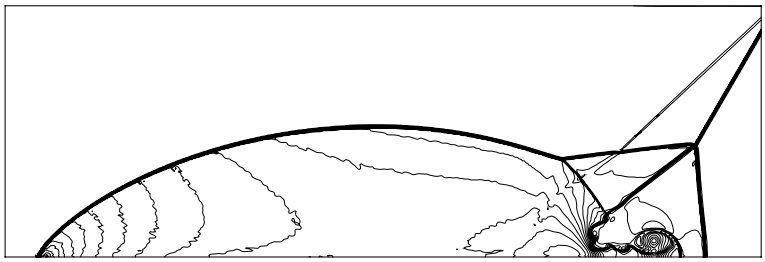

Fig. 4. Density contours of double Mach reflection problem, 50 equally spaced contour levels, 800×200 grid points, $t = 0.2$. Characteristic-wise hybrid compact-WENO scheme, Roe type, with the modified entropy fix , $r_c = 0.4$.

significant influence on the resolution property of the hybrid scheme. Generally speaking, using smaller r_c, higher resolution can be achieved. When r_c is sufficiently small, the numerical results is insensitive to r_c. For example, the numerical results for $r_c = 0.3$ is quite similiar to that for $r_c = 0.218$. However, when we choose $r_c < 0.218$ in this case, negative pressure or density will occur and the computation will break off.

4.2. Double Mach reflection

This is a two-dimensional test case for high resolution schemes [15]. The computational domain for this problem is $[0,4] \times [0,1]$ and a wall lies on the bottom of the computational domain starting from $x = 1/6$. Initially, a right-moving Mach 10 shock is positioned across $(x = 1/6, y = 0)$ and makes a 60° angle with the x-axis. 800×200 grid points are used in the computation. The time step is computed according to

$$\Delta t = \mathrm{CFL}\frac{\Delta t_x \Delta t_y}{\Delta t_x + \Delta t_y},$$

where

$$\Delta t_x = \frac{\Delta x}{\max_{j,k}(|u_{j,k}| + a_{j,k})},$$

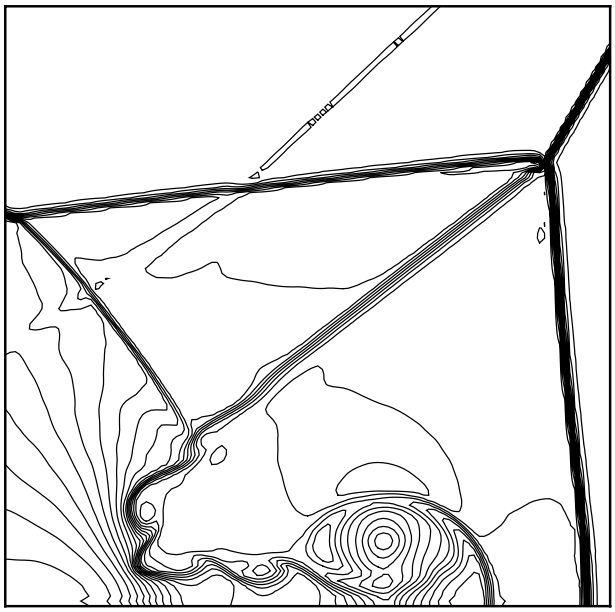

Fig. 5. The enlarged portion of Fig. 4 near the Mach stems.

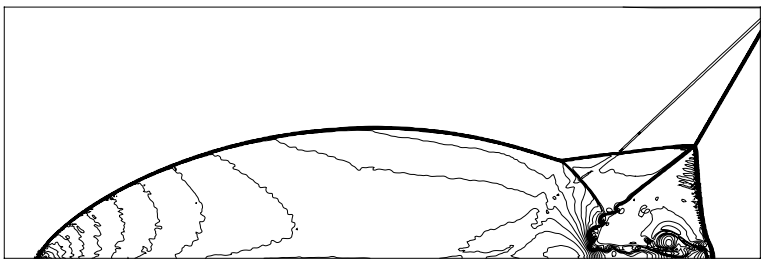

Fig. 6. Density contours of double Mach reflection problem, 50 equally spaced contour levels, 800×200 grid points, $t = 0.2$. Characteristic-wise hybrid compact-WENO scheme, Roe type, with the original entropy fix, $r_c = 0.5$.

$$\Delta t_y = \frac{\Delta y}{\max_{j,k}(|v_{j,k}| + a_{j,k})}.$$

The Courant number is set to CFL = 0.5 in the computation. The solution is advanced in time up to $t = 0.2$.

This test case is difficult for Riemann solver-based flux difference splitting schemes such as Roe scheme because when the grid is fine enough, the "carbuncle phenomenon" will happen near the stronger mach stem that is a nearly normal shock. To cure this problem, the modified H-correction procedure in Eq. (21) is used in the characteristic-wise hybrid compact-WENO scheme. The numerical result of density contours for $r_c = 0.4$ is shown in Figs. 4 and 5. During the computation, the fluxes are computed using the compact scheme on most cell interfaces. The percentage of interfaces on which the WENO fluxes are needed varies from 0.9% to 7.4% at different time. When the original entropy fix in Eq. (20) is used and $r_c = 0.4$, negative density occurs in the numerical solution and the result for $r_c = 0.5$ is shown in Figs. 6 and 7 instead. Even with a larger r_c, the shock instability can still be observed in

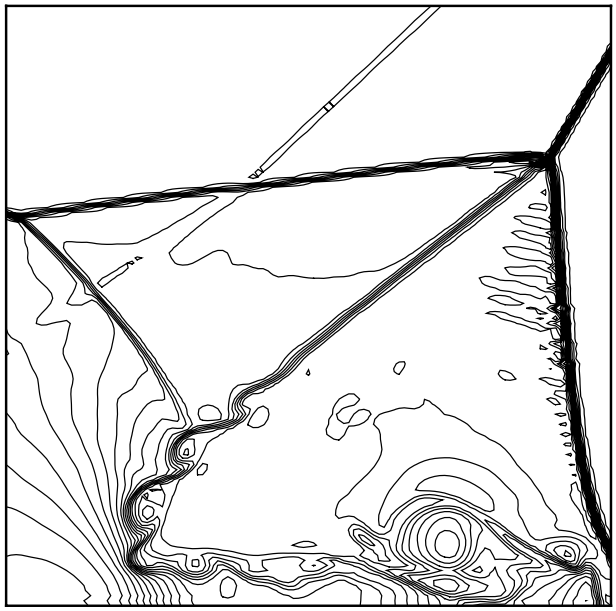

Fig. 7. The enlarged portion of Fig. 6 near the Mach stems.

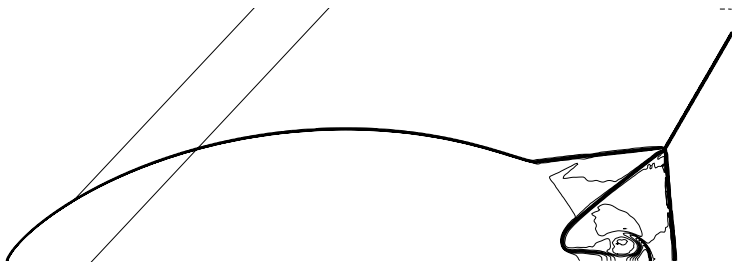

these figures. For the purpose of comparison, the density contours computed using the component-wise hybrid compact-WENO scheme and the WENO scheme with the modified H-correction procedure are depicted in Figs. 8, 9 and 10, 11, respectively. From these figures, it is evident that the characteristic-wise hybrid scheme achieves higher resolution in the numerical results than both the component-wise hybrid scheme and the characteristic-wise WENO scheme, especially in the region near the Mach stems where the characteristic-wise hybrid scheme can capture the rollup of the slip line more clearly. It should be noted that the weight function used in the present component-wise hybrid scheme is Weight B in terms of the density difference for all components which is different with the Pirozzoli scheme. When $r_c = 0.4$, the present component-wise hybrid scheme also produce negative density and the numerical results presented in Figs. 8 and 9 are obtained using $r_c = 0.42$. On the other hand, no negative density and pressure will occur in the numerical solution of the characteristic-wise hybrid scheme even when the threshold value r_c is chosen as smaller as 0.3.

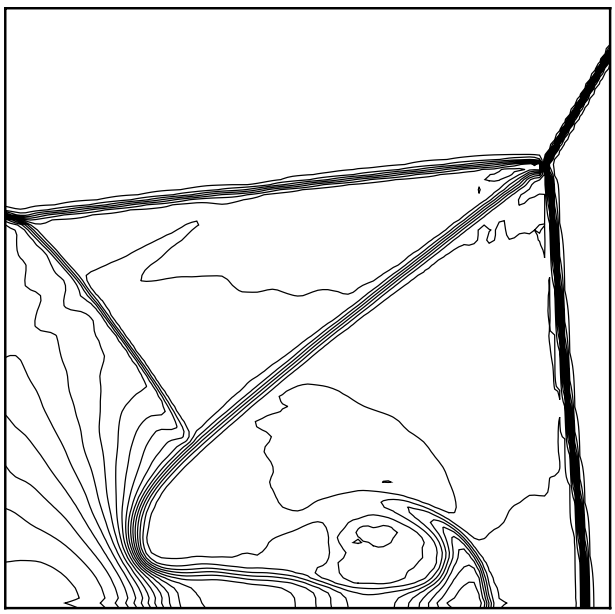

Fig. 9. The enlarged portion of Fig. 8 near the Mach stems.

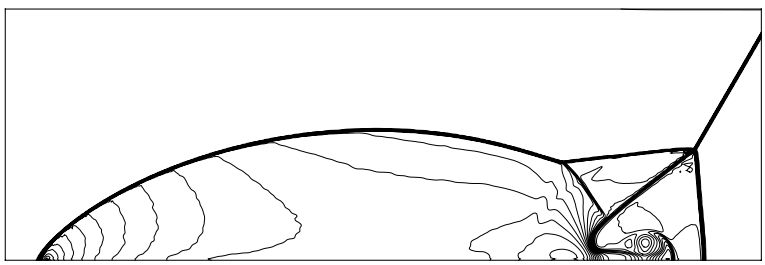

Fig. 10. Density contours of double Mach reflection problem, 50 equally spaced contour levels, 800×200 grid points, $t = 0.2$. Characteristic-wise WENO scheme, Roe type, with the modified entropy fix.

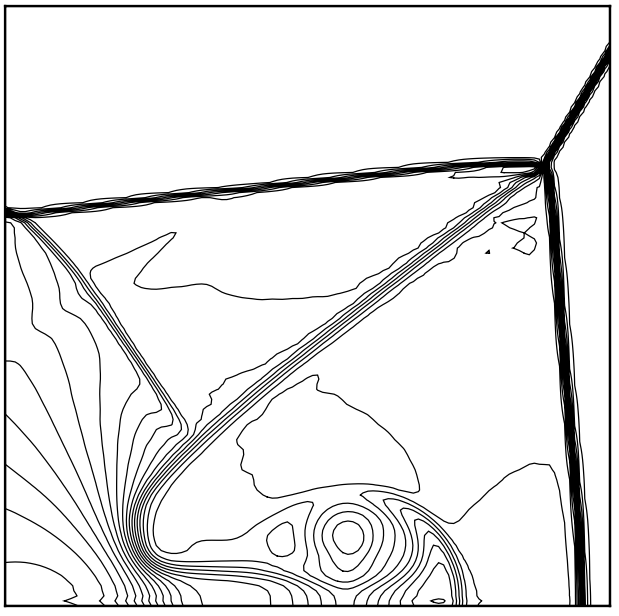

Fig. 11. The enlarged portion of Fig. 10 near the Mach stems.

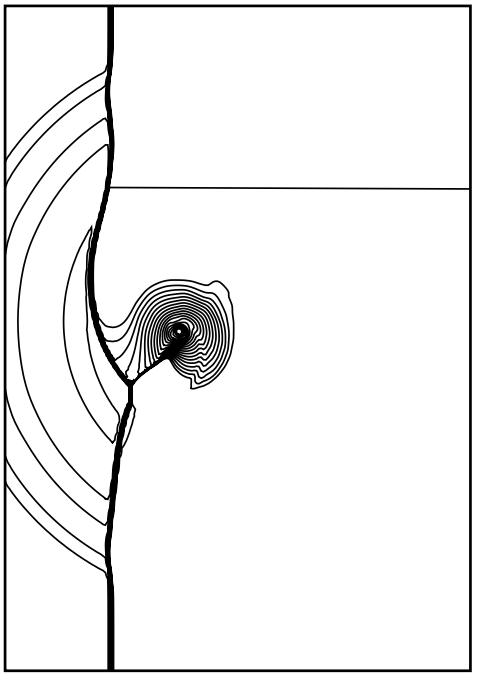

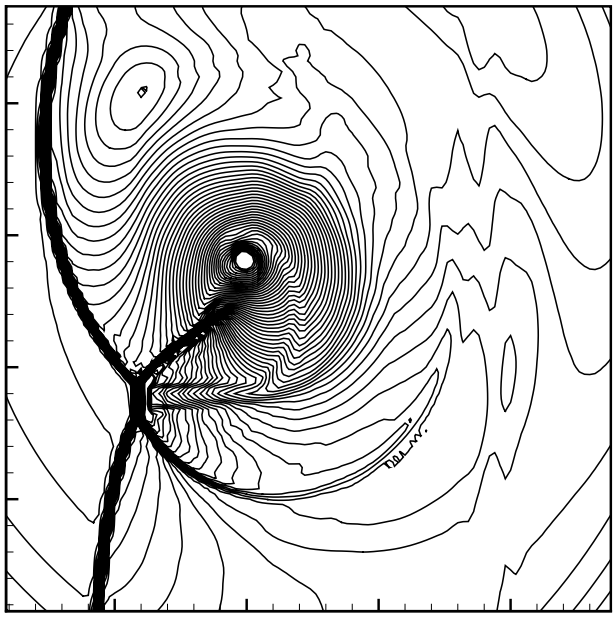

Fig. 13. The enlarged portion of Fig. 12 near the vortex with 60 equally spaced contour levels.

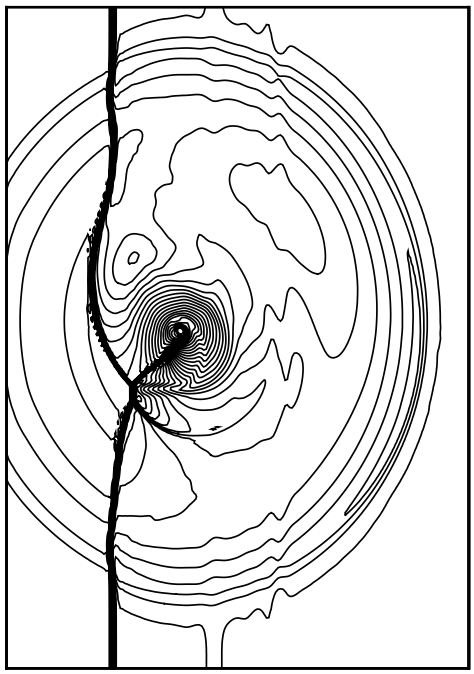

Fig. 14. Density contours of the shock-vortex interaction problem, 30 equally spaced contour levels, 200×300 grid points, $t = 1.538$. Component-wise hybrid compact-WENO scheme, flux splitting type, $r_c = 0.4$.

4.3. The shock–vortex interactions

The flow conditions of this test case are based on [3]. The computational domain is $[-2,2]\times[-3,3]$. At $t=0$, a left-moving Mach 1.5 planar shock is placed at $x=1.66$. Ambient conditions are prescribed to the left of the shock with the velocity being perturbed by a compressible vortex centered at $(x,y)=(0,0)$. To the right of the shock, the flow variables are determined according to the Rankine–Hugoniot relations. The vortex is modeled by

$$U_\theta(r)=\begin{cases} U_c, & r<0.5,\\ 2/3U_c(-r+1/r), & 0.5\leqslant r\leqslant 1,\end{cases}$$

where U_θ is the tangential velocity, r is the distance from the vortex center, and U_c is set to be the velocity behind the shock wave. The characteristic boundary conditions based on the Riemann invariants are used at the left and right boundaries and the periodic conditions are prescribed at the top and bottom boundaries. The domain is discretized into a 200×300 uniform grid. The Courant number is set to CFL $=0.5$.

This test case is computed using the characteristic-wise hybrid compact-WENO scheme ($r_c=0.4$), the component-wise flux splitting hybrid compact-WENO scheme ($r_c=0.4$) and the WENO scheme. The density contours at $t=1.538$ are shown in Figs. 12, 14, and 16, respectively. The enlarged portions of these figures near the vortex center are shown, respectively in Figs. 13, 15, and 17. For the characteristic-wise hybrid scheme, the percentage of interfaces on which the WENO fluxes are needed is around 1.5–2.1% during the simulation. At $t=1.538$, the interactions between the shock wave and the vortex produce a Mach structure. This structure can be correctly captured by all these three schemes. The resolution power of the component-wise hybrid scheme is slightly better than the WENO scheme whereas the characteristic-wise hybrid scheme performs best in resolving the shock waves as well as the contact discontinuities. According to the numerical results, the moving shock can be captured with two

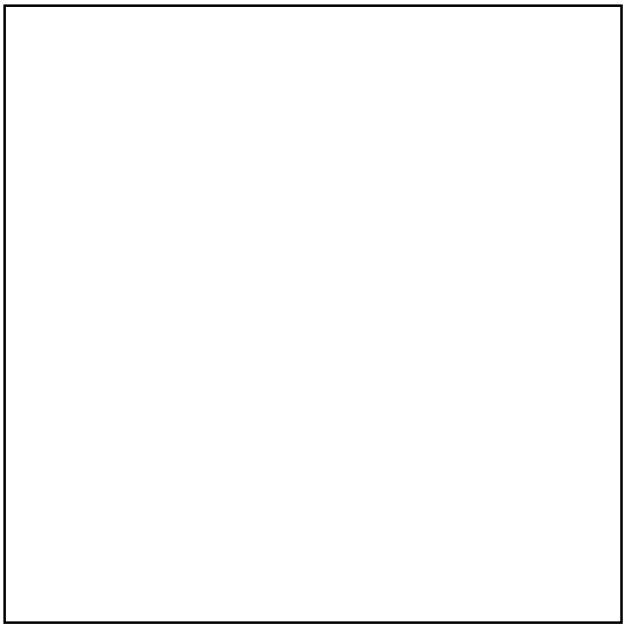

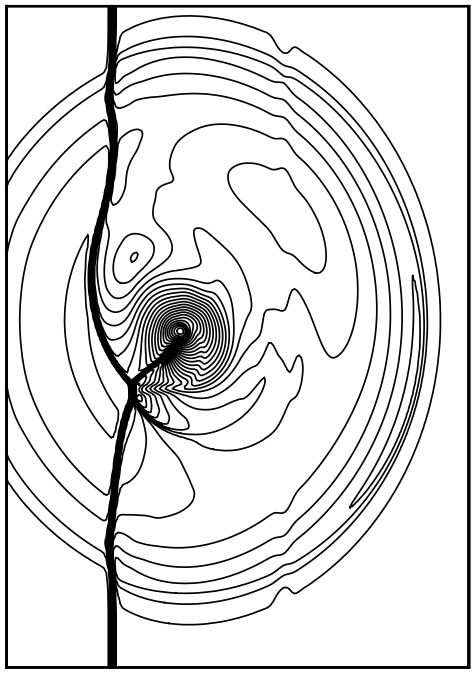

Fig. 16. Density contours of the shock-vortex interaction problem, 30 equally spaced contour levels, 200×300 grid points, $t = 1.538$. Characteristic-wise WENO scheme, Roe type, with the modified entropy fix.

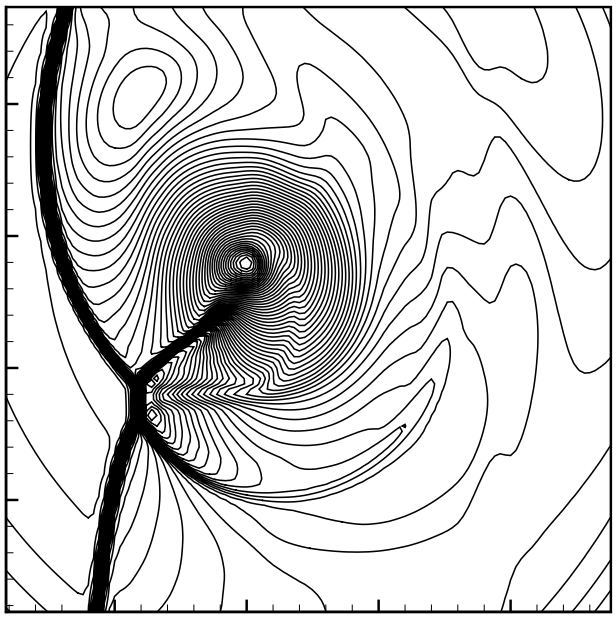

Fig. 17. The enlarged portion of Fig. 16 near the vortex with 60 equally spaced contour levels.

or three cells using the characteristic-wise hybrid scheme and three or four cells are needed by the WENO scheme to resolve this shock wave.

5. Conclusions

In this paper, several improvements have been proposed to the hybrid compact-WENO scheme [10]. Firstly, we consider the hybrid scheme as the weighted average of two sub-schemes: the conservative compact scheme proposed by Pirozzoli [10] and the WENO scheme. A continuous weight function is designed so that the abrupt transition from one sub-scheme to another is avoided. Secondly, when solving a system of hyperbolic conservation laws such as the Euler equations of gas dynamics, a characteristic-wise hybrid compact-WENO scheme is proposed which couples the Roe type, characteristic-wise compact scheme with the Roe type characteristic-wise WENO scheme. Thirdly, in order to remove the entropy violating solutions and the shock instabilities such as the "carbuncle" and the "odd-even decoupling" phenomenon associated with the Roe type scheme, an improved entropy fix procedure is proposed. Numerical tests show a significant improvement in resolution for flows with complex structures over the WENO scheme as well as the component-wise hybrid scheme.

Acknowledgements

This work was supported by the National Natural Science Foundation of China (No. 19972035) and the China NKBRSF (No. 2001CB409600). We thank the referees of this paper for their valuable suggestions to improve the quality of this paper.

References

[1] N.A. Adams, K. Shariff, A high-resolution hybrid compact-ENO scheme for shock-turbulence interaction problems, J. Comput. Phys. 127 (1996) 27.
[2] D. Balsara, C.-W. Shu, Monotonicity preserving weighted essentially non-oscillatory schemes with increasingly high order of accuracy, J. Comput. Phys. 160 (2000) 405.
[3] A. Chatterjee, Shock wave deformation in shock–vortex interactions, Shock Waves 9 (1999) 95.
[4] B. Cockburn, C.-W. Shu, Nonlinearly stable compact schemes for shock calculation, SIAM J. Numer. Anal. 31 (1994) 607.
[5] X. Deng, H. Maekawa, Compact high-order accurate nonlinear schemes, J. Comput. Phys. 130 (1997) 77.
[6] X. Deng, H. Zhang, Developing high-order weighted compact nonlinear schemes, J. Comput. Phys. 165 (2000) 22.
[7] E. Garnier, P. Sagaut, M. Deville, A class of explicit ENO filters with application to unsteady flows, J. Comput. Phys. 170 (2001) 184.
[8] A. Harten, B. Engquist, S. Osher, S. Chakravarthy, Uniformly high order essentially non oscillatory schemes, III, J. Comput. Phys. 71 (1987) 213.
[9] G.S. Jiang, C.-W. Shu, Efficient implementation of weighted ENO schemes, J. Comput. Phys. 126 (1996) 202.
[10] S. Pirozzoli, J. Comput. Phys. 178 (2002) 81.
[11] R. Sanders, E. Morano, M. Druguet, Multidimensional dissipation for upwind schemes: Stability and applications to gas dynamics, J. Comput. Phys. 145 (1998) 511.
[12] C.-W. Shu, High order ENO and WENO schemes for computational fluid dynamics, in: T.J. Barth, H. Deconinck (Eds.), High-Order Methods for Computational Physics, Lecture Notes in Computational Science and Engineering, vol. 9, Springer, Berlin, 1999, pp. 439–582.
[13] C.-W. Shu, S. Osher, Efficient implementation of essentially non-oscillatory shock-capturing schemes II, J. Comput. Phys. 83 (1989) 32.
[14] Z. Wang, G.P. Huang, An essentially nonoscillatory high-order Padé-type (ENO-Padé) scheme, J. Comput. Phys. 177 (2002) 37.
[15] P. Woodward, P. Colella, Numerical simulations of two-dimensional fluid flow with strong shocks, J. Comput. Phys. 54 (1984) 115.
[16] H.C. Yee, N.D. Sandham, M.J. Djomehri, Low-dissipative high-order shock-capturing methods using characteristic-based filters, J. Comput. Phys. 150 (1999) 199.